

Dynamics of flux-line bundles and voltage-current characteristics in a Ba(K)Fe₂As₂ single crystalK.-H. Müller,^{1,*} S. K. H. Lam,¹ X. L. Wang,² and S. X. Dou²¹*CSIRO, Materials Science and Engineering, Sydney, New South Wales 2070, Australia*²*Institute for Superconducting Electronic Materials, University of Wollongong, Wollongong, New South Wales 2522, Australia*

(Received 4 November 2011; revised manuscript received 15 May 2012; published 14 June 2012)

Understanding the flux-line dynamics in layered superconductors is of utmost importance for many superconductor applications, yet extracting from measurements the relevant parameters remains a major challenge. Here we report on measurements and theoretical model calculations of voltage-current (V - I) characteristics of a superconducting Ba_{0.72}K_{0.28}Fe₂As₂ single crystal slightly below its transition temperature in perpendicular magnetic fields between 0.01 and 7 T. We propose a model that describes the flux-line dynamics above, as well as below, the depinning current. The model fits the experimental V - I characteristics remarkably well and is used to extract from the data the field dependence of (a) the depinning current, (b) the pinning potential barrier height, (c) the dissipative resistance, and (d) the product between flux-line bundle volume and bundle hopping distance. The model also leads to an estimate of the average distance between pins.

DOI: [10.1103/PhysRevB.85.224516](https://doi.org/10.1103/PhysRevB.85.224516)

PACS number(s): 74.25.-q, 74.70.Xa, 74.25.F-, 74.25.Wx

I. INTRODUCTION

When a type-II superconductor is exposed to a magnetic field larger than its lower critical field and a sufficiently large electric current is applied, depinning of the Abrikosov flux-line lattice occurs. By measuring the dc voltage-current (V - I) characteristics of a superconductor and by applying a detailed theoretical model, one can elucidate the dynamics of flux-line depinning, which is of great importance for many small- and large-scale superconductor applications. While magnetization loop and flux-creep measurements explore the realm of small electric fields, where the flux-line motion is very slow, V - I characteristics in general probe flux dynamics in the realm of large electric fields generated by the fast motion of flux lines.

Flux-line lattice dynamics in cuprate superconductors have been studied extensively both experimentally and theoretically.^{1–20} Very recently different groups have started to investigate the flux-line lattice dynamics in the newly discovered iron pnictide superconductors.^{21–27} Among the pnictides, the hole-doped Ba(K)Fe₂As₂ superconductor is one of several known iron pnictide superconductors, which we have investigated previously by magnetization loop and resistive transition measurements.²⁷ Ba(K)Fe₂As₂ has been found to be a two-band superconductor,^{28,29} and the material consists of an alternating structure of FeAs and Ba(K) layers with a spacing of ~ 0.65 nm.³⁰ As the Ba layers are doped with K atoms, they donate carriers to the covalently bonded FeAs layers and suppress the global antiferromagnetism, causing superconductivity to appear. The Ba(K)Fe₂As₂ layered structure is reminiscent of the structure of cuprates and suggests that the superconducting behavior of iron pnictides may have similarities with the some of the cuprates. Importantly, Ba(K)Fe₂As₂ single crystals show relatively low magnetic anisotropy, which is advantageous for applications.²⁷ Although much has been learned about the flux-line dynamics in layered superconductors, extracting in a simple way from measurements the relevant parameters remains a major challenge.

In this paper we present measurements and theoretical model calculations of V - I characteristics of a

Ba_{0.72}K_{0.28}Fe₂As₂ single crystal slightly below the transition temperature in magnetic fields between 0.01 and 7 T, applied along the crystallographic c direction. Crystals from the same batch had been characterized previously²⁷ by magneto-optical imaging and high-resolution transmission electron microscopy (TEM) and TEM diffraction patterns and were found to be of high quality, i.e., without indications of microcracks, weak links, or crystal defects. Although our experimental investigations limit themselves to a single temperature close to the critical temperature, a wide field range is covered. Giving the steepness of the irreversibility line in this material,³¹ one can expect that relevant pinning regimes will be covered. The theoretical model for the V - I characteristics, which we use describes the flux-line dynamics at arbitrary drive currents, i.e., below and above the depinning current. In the model the Johnson white-noise current in the two-band material induces thermally activated flux-line bundle hopping at drive currents below the depinning current, while for drive currents above the depinning current, resistively damped flux motion occurs. At small drive currents, our model is equivalent to the thermally assisted flux flow (TAFF) model. But, our model goes beyond the TAFF approach, as it also describes the motion of flux lines at currents close to and larger than the depinning current. We show that the model fits the measured V - I characteristics remarkably well over the full current range, at all magnetic fields investigated. The model allows us to extract from the experimental data the magnetic field dependence of (a) the depinning current, (b) the barrier height of the pinning potential, (c) the dissipative resistance, and (d) the product between bundle volume and hopping distance. The model also enables us to estimate the average distance between pins.

In Sec. II we give details about the experiment procedure, and in Sec. III we outline the theoretical model. In Sec. IV we compare our measured V - I characteristics with our model calculations and extract from the data the depinning current, the pinning potential barrier height, the dissipative resistance, the product between flux-line bundle volume and hopping distance, and estimate the distance between pins. The conclusion is given in Sec. V.

II. EXPERIMENTAL DETAILS

The $\text{Ba}_{0.72}\text{K}_{0.28}\text{Fe}_2\text{As}_2$ single crystal was grown using a flux method where high-purity elemental Ba, K, Fe, As, and Sn were mixed in a molar ratio of $(\text{Ba}_{1-x}\text{K}_x\text{Fe}_2\text{As}_2):\text{Sn} = 1:45\text{--}50$ for the self-flux. Details of the crystal growth are given in Ref. 32. We have shown previously by magneto-optical imaging²⁷ that such crystals are of high magnetic uniformity. The $\text{Ba}_{0.72}\text{K}_{0.28}\text{Fe}_2\text{As}_2$ crystal that we have investigated here was taken from the same batch as the crystals studied in Ref. 27. Our $\text{Ba}_{0.72}\text{K}_{0.28}\text{Fe}_2\text{As}_2$ single crystal had the approximate dimensions $1.5 \times 1.0 \times 0.02 \text{ mm}^3$ and was glued onto a MgO substrate using polyimide. The single crystal was cleaved to obtain a fresh surface and current, and voltage contacts were made in a four-point probe configuration, applying conductive silver paint such that the drive current could flow along the crystallographic ab direction. We have measured the dc V - I characteristics of the $\text{Ba}_{0.72}\text{K}_{0.28}\text{Fe}_2\text{As}_2$ single crystal in magnetic fields from $B = 0.01 \text{ T}$ up to 7 T , applied along the crystallographic c direction of the crystal, i.e., perpendicular to its layered structure (i.e., perpendicular to the flat side of the crystal). The apparatus used for the measurements was a commercial Quantum Design Physical Property Measurement System (PPMS). The temperature chosen was $T = 31 \text{ K}$, which is about 2° below the zero-field superconducting transition temperature $T_c \approx 33 \text{ K}$ (onset) of the crystal. Lower temperatures were not investigated because the large critical currents would have caused unacceptable self-heating of the crystal. In order to avoid self-heating, the current I was applied only over a short time intervals of $t_p = 20 \text{ ms}$ while the dc voltage V was measured.

III. THEORETICAL MODEL

When a magnetic field greater than the lower critical field is applied to a type-II superconductor, flux lines in the form of Abrikosov vortices form inside the superconductor, where each vortex carries one flux quantum Φ_0 . A drive current applied to the superconductor exerts a Lorentz force on the flux lines, pulling the lines sideways, perpendicular to both the direction of the lines and the direction of the current. If the current is sufficiently large, the Lorentz force will be able to depin the flux lines that are otherwise pinned by defects, i.e., regions of reduced order parameter. When flux lines start to move, a voltage will appear along the sample. As originally proposed by Anderson,¹ the flux-line lattice will not move collectively as a whole but instead correlated regions of flux lines, so called flux-line bundles, will slip past each other, more or less independently in an irregular fashion, over energy barriers of average height U_0 between local energy minima.⁵ The flux-line bundle volume V_b can be defined by its three correlation lengths, l_x , l_y , and l_z , along the different spatial directions, where z is the direction of the applied magnetic field B , and $V_b = l_x l_y l_z$ as shown in Fig. 1. Here the z direction is the crystallographic c direction, and the xy plane corresponds to the crystallographic ab plane of the crystal. The dependence of the correlation lengths on B depends on the elasticity of the flux-line lattice and the distribution and size of the pins. The correlation length in z direction, l_z , cannot be larger than the thickness h of the crystal, and the smallest possible

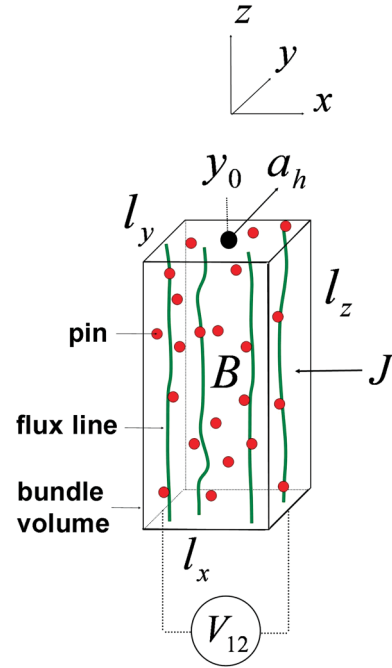


FIG. 1. (Color online) Schematic of a flux-line bundle of volume $V_b = l_x l_y l_z$ at position y_0 with four flux lines inside the bundle, attached to some pins. The applied magnetic field B points in the z direction (crystallographic c direction). The xy plane corresponds to the crystallographic ab plane. The drive current density J points in negative x direction and flows into the area $l_y l_z$. The Lorentz force pulls the bundle in the y direction by the hopping distance a_h . The voltage across l_x is V_{12} .

xy surface area of a bundle is $l_x l_y = \Phi_0/B$, in which case the bundle contains only a single flux line.

We choose the coordinate system such that the applied drive current flows along the negative x direction (Fig. 1). The current density, J , that passes through the bundle (Fig. 1), exerts a Lorentz force on the bundle, pulling the bundle sideways (in the y direction) against the pinning force generated by the pins. When a bundle with coordinate y_0 moves in the y direction, the work W that is supplied externally by the electrical power supply to the bundle is

$$W(y_0) = J B V_b y_0 - U(y_0). \quad (1)$$

Here $U(y_0)$ is the pinning potential of the bundle. Because the actual shape of the pinning potential manifold is not known, we assume for simplicity that $U(y_0)$ is of sinusoidal shape. Denoting by a_h the flux-line bundle hopping distance (Fig. 1), one can write

$$U(y_0) = \frac{U_0}{2} [1 - \cos(2\pi y_0/a_h)], \quad (2)$$

where U_0 is the barrier height of the pinning potential. In Eq. (1), we have neglected the kinetic energy term from the motion of the bundle, by assuming strong dissipative damping of the bundle from the normal electrical resistance inside the bundle volume.

The work $W(y_0)$ given by Eq. (1) has the shape of a “washboard” potential, where the current density J tilts $W(y_0)$. The value of J at which $W(y_0)$ ceases to have minima and maxima defines the “true” critical current density J_c , which is

commonly called the depinning current density. One finds

$$U_0 = J_c B V_b a_h / \pi. \quad (3)$$

Equation (3) relates the barrier height U_0 of the pinning potential to the depinning current density J_c , the flux-line bundle volume V_b , and the bundle hopping distance a_h .

From Eqs. (1) and (2), it follows that the power P_{in} , which is delivered by an external current source to the volume V_b , is given by

$$P_{in} = \frac{\partial W}{\partial t} = J B V_b \partial y_0 / \partial t - \frac{\pi U_0}{a_h} \frac{\partial y_0}{\partial t} \sin(2\pi y_0 / a_h). \quad (4)$$

The motion of a flux-line bundle in the y direction generates an electric field $E_x = B \partial y_0 / \partial t$ in the x direction inside the bundle, which gives rise to a resistive power dissipation inside the bundle. The voltage $V_{12}(t)$ generated across the bundle along the x direction (Fig. 1) is given by

$$V_{12}(t) = l_x B \frac{\partial y_0}{\partial t}. \quad (5)$$

Thus, the power, P_{diss} , which is dissipated inside the bundle volume V_b is

$$P_{diss} = \frac{V_{12}^2}{R_b} = \frac{l_x^2 B^2 (\partial y_0(t) / \partial t)^2}{R_b}, \quad (6)$$

where R_b is the electrical resistance from normal electron scattering inside the bundle volume.

By equating Eq. (4) with Eq. (6), i.e., $P_{in} = P_{diss}$, one obtains a nonlinear differential equation for $y_0(t)$ of the form

$$\frac{l_x B}{R_b} \frac{\partial y_0}{\partial t} + I_{bc} \sin(2\pi y_0(t) / a_h) = I_b + \tilde{I}_b(t). \quad (7)$$

Here I_b is the drive current that flows along the x direction through the bundle volume V_b , i.e., $I_b = J l_y l_z$, and I_{bc} is the bundle depinning current, $I_{bc} = J_c l_y l_z$. Most importantly, on the right side of Eq. (7) we have added to the dc drive current I_b the term $\tilde{I}_b(t)$, which is the Johnson white-noise current,³³ originating from thermal fluctuations in the electrical resistance R_b inside the volume V_b . The Johnson white-noise current $\tilde{I}_b(t)$ is defined via its autocorrelation function

$$\langle \tilde{I}_b(t + \tau) \tilde{I}_b(t) \rangle_t = \frac{2k_B T}{R_b} \delta(\tau), \quad (8)$$

where k_B is the Boltzmann constant, $\delta(\tau)$ the delta function, T the temperature, and $\langle \cdots \rangle_t$ means time averaging. It is important to notice that the Johnson white-noise current $\tilde{I}_b(t)$ gives rise to the thermally activated hopping of flux-line bundles, which leads to the appearance of a finite voltage along the superconductor even at current densities J smaller than the depinning current density J_c . Equation (7) above has the same mathematical form as the equation that describes a resistively shunted Josephson junction (RSJJ) with current noise.^{33,34} In the RSJJ equation the noise current is the Johnson white noise of the junction resistance and the sine term is due to the interference of the order parameter of two superconductors in proximity. In contrast, in Eq. (7), the sine term arises from the simple sinusoidal pinning potential that was assumed. A

model nearly identical to Eq. (7) had been proposed previously by Coffey *et al.*,³⁵ where it was used to describe the rf surface impedance of type-II superconductors.

The dc voltage V between two contact points spaced a distance L apart along the x direction, is given by summing up all the voltages across all the bundles and time averaging them. Thus,

$$V = \frac{L}{l_x} \langle V_{12}(t) \rangle_t. \quad (9)$$

From Eqs. (5), (7), and (9), one finds that the V - I characteristics can be calculated as

$$V = R(B, T) [I - I_c(B, T) \langle \sin(2\pi y_0(t) / a_h) \rangle_t], \quad (10)$$

where I is the total drive current applied through the crystal, i.e.,

$$I = I_b \frac{wh}{l_y l_z}, \quad (11)$$

where w is the width, h the thickness of the crystal, and $I_c(B, T)$ is the total depinning current, i.e., $I_c(B, T) = J_c(B, T)wh$, and $R = R_b L l_y l_z / (l_x w h)$.

We estimate the dissipative resistance $R(B, T)$ in Eq. (10) by taking the two band structures of Ba(K)Fe₂As₂ into account, which has been shown to have a small and a large superconducting gap.^{28,29} Assuming that at a measuring temperature slightly below T_c , the smaller gap is still closed, one obtains, according to the model by Goryo *et al.*³⁶

$$R(B, T) = \frac{B}{B_{c2}(T) / R_n^{(L)}(T) + B / R_n^{(S)}(T)} \quad \text{for } B \leq B_{c2}(T),$$

and

$$R(B, T) = R(B_{c2}, T) \quad \text{for } B \geq B_{c2}(T). \quad (12)$$

Here $R_n^{(S)}(T)$ and $R_n^{(L)}(T)$ are the normal resistances originating from the two bands, which have small (S) and large (L) superconducting gaps at the Fermi surfaces. In the limit $R_n^{(S)} / R_n^{(L)} \rightarrow \infty$, Eq. (12) becomes the Bardeen-Stephen flux-flow resistance, while for $R_n^{(S)} / R_n^{(L)} \rightarrow 0$, one finds $R(B, T) = R_n^{(S)}(T)$.

Equation (10) shows that in order to calculate the dc V - I characteristics, one has to first solve Eq. (7) by taking the noise current $\tilde{I}_b(t)$ into account, and then one has to calculate the time-averaged quantity $\langle \sin(2\pi y_0(t) / a_h) \rangle_t$.

We have solved Eq. (10) by using two methods that were previously developed to solve the RSJJ equation. The first method is described by Likharev³⁷ and the second by Voss.³³ In the method discussed by Likharev,³⁷ one solves the corresponding Fourier-transformed Smoluchowski equation,³⁴ which gives

$$\langle \sin(2\pi y_0(t) / a_h) \rangle_t = \text{Re } \sigma_1, \quad (13)$$

where σ_1 is determined iteratively from

$$2(I / I_c - ik\gamma) \sigma_k + \sigma_{k-1} + \sigma_{k+1} = 0. \quad (14)$$

Here

$$\gamma = \frac{U_0}{k_B T}, \quad (15)$$

i is the imaginary unit, $\sigma_0 = 1$, and the integer index $k > 0$ can be cut off at $k \gg 1$ as σ_k tends to zero monotonically as $k \rightarrow \infty$.

A subtle point to notice is that in our case the parameter γ defined by Eq. (15) is not given by $\Phi_0 I_{bc}/(\pi k_B T)$ as one might expect in equivalence to the RSJJ model. This becomes clear if one writes Eq. (7) in the form of the RSJJ model, i.e.,

$$\frac{\Phi_0}{2\pi \tilde{R}} \frac{\partial \varphi(t)}{\partial t} + I_{bc} \sin(\varphi(t)) = I_b + \tilde{I}_b(t), \quad (16)$$

where $\varphi(t) \equiv 2\pi y_0(t)/a_h$ and $\tilde{R} \equiv R_b \Phi_0/(l_x B a_h)$. It is of importance to note here that \tilde{R} is not equal to R_b and that R_b , and not \tilde{R} , determines the noise current $\tilde{I}_b(t)$, as seen from Eq. (8). This is in contrast to the RSJJ model, where $\tilde{R} = R_b$, R_b then being the ohmic resistance of the Josephson junction.

As an alternative second method to solve Eq. (7), we have also used the numerical method described by Voss.³³ In this method the noise current $\tilde{I}_b(t)$ is treated as a Gaussian random variable of mean-square deviation $2k_B T/(R_b \Delta t)$, where Δt is the integration time step, and then the time-averaged quantity $\langle \sin(2\pi y_0(t)/a_h) \rangle_t$ is computed. With both methods, Likharev³⁷ and Voss,³³ we obtain the same results. While the method by Voss is computationally more demanding, it has the advantage that one can study the random hopping of bundles on a very short timescale and can investigate voltage fluctuations before one time averages the voltage.

It should be noted that without the Johnson white-noise current \tilde{I}_b in Eq. (7), the V - I characteristics would have the simple form

$$V = R(I^2 - I_c^2)^{1/2}, \quad (17)$$

for $I \geq I_c$, and $V = 0$ otherwise.

For $I < I_c$ and for large γ , an analytical solution can be found for Eqs. (7) and (10),³² which is of the form

$$V = 2RI_c(1 - x^2)^{1/2} \exp \left\{ -\frac{U_0}{kT}((1 - x^2)^{1/2} + x \arcsin x) \right\} \times \sinh \left(\frac{\pi U_0}{2kT} x \right), \quad (18)$$

where $x = I/I_c$. For $I \ll I_c$, one finds from Eq. (18)

$$V = 2RI_c \exp \left\{ -\frac{U_0}{kT} \right\} \sinh \left(\frac{\pi U_0}{2kT} x \right), \quad (19)$$

which is the TAFF model.⁸ Furthermore if $\pi U_0 x/(2kT) \ll 1$, then

$$r \equiv \frac{V}{I} = \pi \frac{U_0}{kT} R \exp \left\{ -\frac{U_0}{kT} \right\}. \quad (20)$$

Equation (20) is commonly used to estimate $U_0(B)$ from measurements of the resistance r versus temperature around the transition temperature. By plotting the experimental $\ln r$ versus $1/T$, and neglecting the weak temperature dependence of the prefactor in Eq. (20), U_0 can be extracted. One has to be aware that this method assumes that U_0 can be written as a product between a field and a temperature-dependent function, where the temperature part must have the special form $(1 - T/T_c)$. In contrast, when extracting U_0 from experimental V - I characteristics with our model, i.e., by using Eqs. (7) and

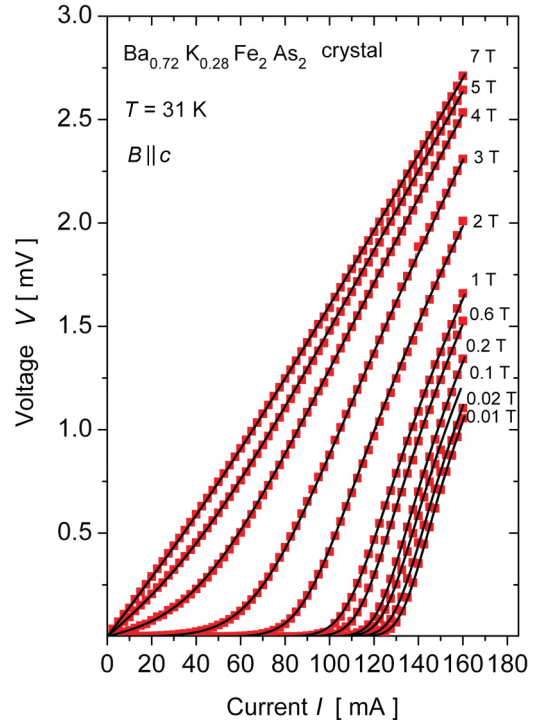


FIG. 2. (Color online) Measured V - I characteristics (squares) of a $\text{Ba}_{0.72}\text{K}_{0.28}\text{Fe}_2\text{As}_2$ single crystal with $T_c \approx 33$ K at $T = 31$ K in magnetic fields from $B = 0.01$ to 7 T applied along the c direction. The full curves are the calculated results, using the model outlined in Sec. III.

(10), no assumption has to be made about the temperature dependence of U_0 . Also, it is generally difficult to extract with the TAFF model Eq. [(19)] the depinning current I_c as the TAFF model is valid only for $I \ll I_c$. Also, in low fields the voltage often becomes unmeasurably small when $I \ll I_c$. In contrast, our model allows one to extract U_0 and I_c in an accurate and straightforward way. The field dependence of U_0 and I_c can then be used to determine the field dependence of the product, $V_b a_h$, between flux bundle volume V_b and hopping distance a_h .

In the limit $I_b \rightarrow 0$, our model [Eq. (7)] resembles the model that was introduced by Tinkham⁵ to describe the field dependence of the resistive transition of cuprate superconductors measured at a small drive current.

IV. RESULTS AND DISCUSSION

Figures 2 and 3 show the measured dc voltage V versus the applied dc current I (V - I characteristics) for 11 different magnetic fields B between 0.01 and 7 T, applied perpendicular to the sample along the crystallographic c direction. The temperature was kept constant at $T = 31$ K, which is about 2° below the zero-field transition temperature of the crystal. Figure 3 shows the same experimental data and calculated curves as Fig. 2 but now in the form of $\log V$ versus I . As can be seen from Fig. 2, the V - I characteristics do not show Bardeen-Stephens flux-flow behavior where one would expect curves of convex shape with slopes that increase with increasing applied magnetic fields. Instead, the V - I characteristics in Fig. 2 show a gradually transition in shape from convex to concave, and for large currents the voltage

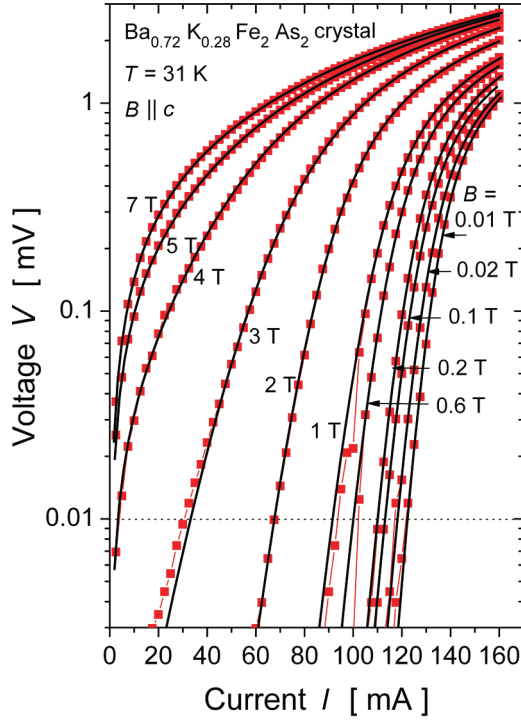


FIG. 3. (Color online) Same as in Fig. 2 but as a log V versus I plot, i.e., measured V - I characteristics of a $\text{Ba}_{0.72}\text{K}_{0.28}\text{Fe}_2\text{As}_2$ single crystal at $T = 31$ K in magnetic fields from $B = 0.01$ to 7 T applied along the c direction. The squares are the measured data, and the full lines are the calculated results, using the model outlined in Sec. III.

seems to approach asymptotically an ohmic behavior, i.e., $V \sim I$. At $B = 7$ T, close to ohmic behavior is observed over the entire current range. The shapes of the V - I characteristics resemble V - I characteristics commonly seen in RSJJ and in single crystals of high-temperature cuprate superconductors, where in the case of the cuprates, the low current range is often interpreted as TAFF behavior.⁸

In order to avoid self-heating of our sample, we used a pulse method where, for each data point, the current I was applied only for a short duration of $t_p = 20$ ms, while the dc voltage V was measured, and the maximum current applied was limited to 160 mA. The time between pulses was chosen as $t_w = 10$ s to allow full temperature equilibration. In order to investigate self-heating of our sample, we performed V - I measurements at longer pulse durations t_p . For the longer times $t_p = 40$ ms and $t_p = 60$ ms, we found the same V - I characteristics, while deviations due to self-heating became evident at $t_p = 80$ ms.

The equations derived in Sec. III show that in order to calculate the V - I characteristics, one needs to know (a) the depinning current density $J_c(B)$, (b) the barrier height $U_0(B)$ of the pinning potential, and (c) the dissipative resistance $R(B)$. As the type of pins and the pin distribution in our crystal are unknown, one cannot estimate J_c and U_0 simply by model calculations. Also, according to Eq. (12), to estimate the resistance R , both the values for $R_n^{(S)}$ and $R_n^{(L)}$ have to be known. Therefore, J_c , U_0 , and R are best being treated as parameters that can be extracted by fitting our model to our measured V - I characteristics.

The full curves in Figs. 2 and 3 show our calculated V - I characteristics for different magnetic fields B pointing along

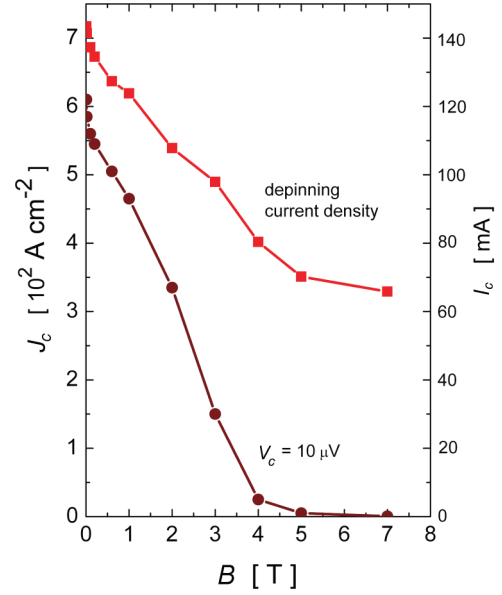


FIG. 4. (Color online) Extracted depinning current density J_c (and depinning current I_c) versus applied magnetic field B . Also shown is the critical current density (critical current) for a voltage criterion $V_c = 10 \mu\text{V}$ obtained from Fig. 3. Here $T = 31$ K.

the crystallographic c direction. The extracted fit parameters J_c , U_0 , and R for the 11 different B fields are shown in Figs. 4–6. As can be seen from Figs. 2 and 3, the calculated V - I characteristics agree remarkably well with our experimental data not only in the TAFF regime but also in the flux-line flow regime at drive currents larger than I_c .

As can be seen in Fig. 4, the extracted depinning current density J_c (and depinning current I_c) decreases with increasing applied magnetic field B . Also shown in Fig. 4 is the critical current density obtained by using the voltage criterion $V_c = 10 \mu\text{V}$ (dashed horizontal line in Fig. 3). Figure 4 reveals that at large fields, a critical current density defined via a common voltage criterion can be very much smaller than the depinning current density J_c (“true” critical current density). The reason is that due to the Johnson white noise, the motion of flux-line bundles becomes thermally activated leading to the appearance of a finite voltage even for $J < J_c$.

By measuring the critical current density of $\text{Ba}(\text{K})\text{Fe}_2\text{As}_2$ single crystals by means of magnetization loops, one finds a fishtail behavior^{38–40} whose origin is not yet fully understood but might be caused by different creep rates in different pinning regimes. In contrast, no fishtail behavior is seen in the depinning current of our Fig. 4. We believe that this is not necessarily contradictory, because a magnetically determined critical current density is strongly affected by the flux-creep rate, which depends on the magnetic field and the pinning regime, while the depinning current density itself is independent of any flux-creep rate.

Figure 5 shows the extracted pinning potential barrier height U_0 in units of $k_B T$ versus the applied magnetic field B where U_0 decreases rapidly with increasing magnetic field. Since $k_B T = 2.67$ meV at $T = 31$ K, the largest value of U_0 is 0.23 eV. The small values of U_0 at large magnetic fields explain the large difference seen between the “true” and the voltage criterion-related critical current densities shown in Fig. 4.

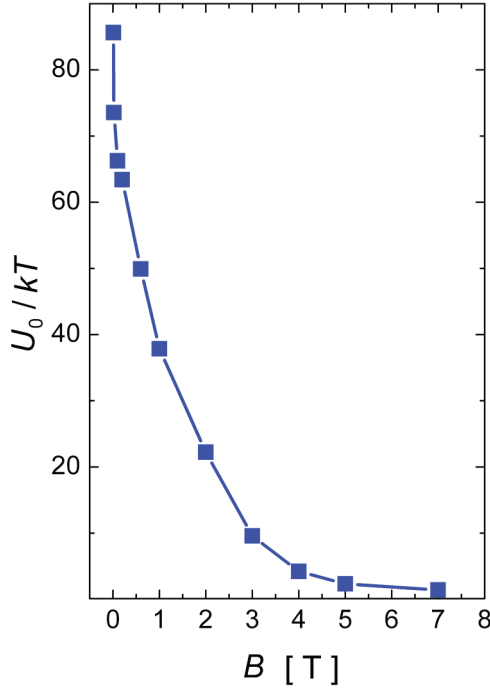


FIG. 5. (Color online) Extracted pinning potential barrier height U_0 in units of $k_B T$ versus the applied magnetic field B . Here $T = 31$ K.

Figure 6 shows the extracted resistance R versus the applied magnetic field B . The resistance is reduced by $\sim 20\%$ at low fields compared to high fields. The full curve in Fig. 6 is a fit using Eq. (12) and assuming $B_{c2}(31\text{K}) = 10$ T. From this fit, one obtains $R_n^{(S)} = 0.015 R_n^{(L)}$. Here, according to Eq. (12), the Bardeen-Stephen flux-flow behavior is strongly suppressed by the small $R_n^{(S)}/R_n^{(L)}$ ratio.

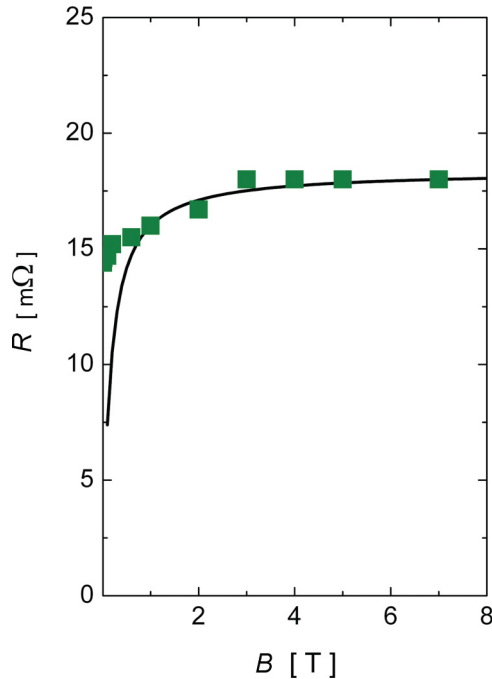


FIG. 6. (Color online) Extracted resistance R versus the applied magnetic field B . The full line shows a fit through the data using Eq. (12). Here $T = 31$ K.

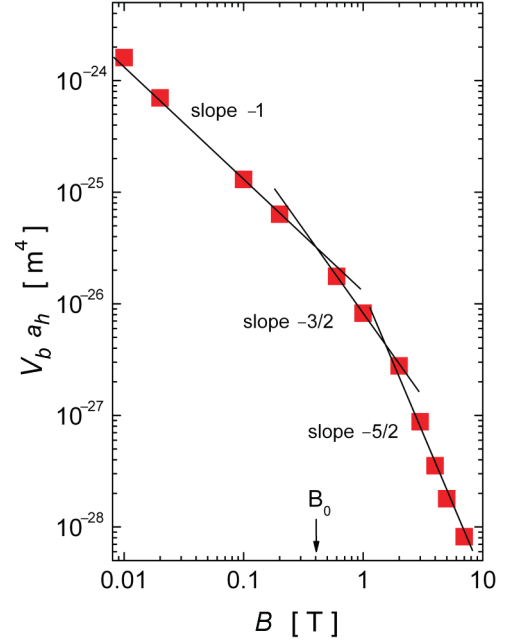


FIG. 7. (Color online) Product $V_b a_h$ between flux bundle volume V_b and hopping distance a_h versus applied magnetic field B . B_0 is the field where slope -1 and slope $-3/2$ cross. Here $T = 31$ K.

We can now use the barrier height U_0 in Fig. 5 and the depinning current J_c in Fig. 4 to determine the product, $V_b a_h$, between the flux-line bundle volume V_b and the hopping distance a_h , since

$$V_b a_h = \frac{\pi U_0}{J_c B}. \quad (21)$$

The extracted dependence of $V_b a_h$ on B is displayed in Fig. 7 as $\log V_b a_h$ versus $\log B$. Figure 7 shows a slope of -1 at small fields and a slope of about $-5/2$ at high fields. One can also assign a slope of $-3/2$ to the intermediate field range as shown in Fig. 7.

The different slopes seen in Fig. 7 can be interpreted as follows:

Bitter decoration experiments at small fields have revealed that the flux-line lattices in iron pnictide single crystals are strongly disordered.⁴¹ Kes⁸ has argued that in the case of a disordered flux-line lattice, the transverse correlation lengths l_x and l_y are best to be chosen as $l_x = l_y = a_f$, where $a_f = (\Phi_0/B)^{1/2}$, which is the average spacing between flux lines. Thus, we assume that in small fields the flux-line bundle volume has the form

$$V_b = a_f^2 l_z(B), \quad (22)$$

which contains just one flux line. If the average distance D between pins is less than a_f , one can estimate for the hopping distance a_h that $a_h = D$. If one further assumes that in small fields $l_z = h$, where h is the thickness of the crystal, one obtains

$$V_b a_h = \frac{\Phi_0 h D}{B}, \quad (23)$$

which explains the observed slope -1 behavior for low fields in Fig. 7.

As the field increases, at a certain field the flux-line lattice spacing a_f will become larger than the average spacing D between pins and then the hopping distance a_h can best be equated with the flux-line lattice spacing a_f .⁸ Also, for any pin distribution, as long as $B > 0.2B_{c2}$, the periodicity of the pinning potential will be that of the sinusoidal variation of the superconducting order parameter, and one can set $a_h = a_f$. In this case one obtains

$$V_b a_h = \frac{\Phi_0^{3/2} h}{B^{3/2}}, \quad (24)$$

which explains the $-3/2$ slope observed for intermediate fields in Fig. 7. In order to obtain the correct magnitude for $V_b a_h$, using $h = 20 \mu\text{m}$ for the thickness of the crystal in Eq. (24), we find that not one but about four flux lines make up a bundle. Therefore, an additional factor of 4 should be included on the right sides of Eqs. (23) and (24), and the above assumption of $l_x = l_y = a_f$ has to be replaced by $l_x = l_y = 2a_f$. Defining B_0 as the field where the slope of -1 goes into slope $-3/2$ in Fig. 7, one finds $B_0 \approx 0.4 \text{ T}$, and from $D = (\Phi_0/B_0)^{1/2}$ one finds $D \approx 70 \text{ nm}$ for the average distance between pins. We speculate that these pins might be due to order parameter fluctuations caused by a nonuniform K dopant distribution in the crystal.⁴² Interestingly, Demiridis *et al.*⁴³ found a similar distance of $\approx 60 \text{ nm}$ between strong pins in $\text{Ba}(\text{Fe}_{1-x}\text{Co}_x)_2\text{As}_2$ single crystals, which was ascribed to order parameter fluctuations caused by nonuniform Co dopant distributions in their crystals.

For large fields, using the concept of collective pinning,^{8,44} one can estimate l_z as

$$l_z \approx \left(\frac{\Phi_0^4 (1 - B/B_{c2})^2}{\mu_0^2 \lambda^4 \bar{W}} \right)^{1/3}, \quad (25)$$

where for the case of flux-line pinning at randomly distributed defects

$$\bar{W} \sim B^3 (1 - B/B_{c2})^2. \quad (26)$$

Replacing in Eq. (24) h by l_z and using Eqs. (25) and (26) leads to

$$V_b a_h \sim B^{-5/2}. \quad (27)$$

We also measured the I - V characteristics of a second $\text{Ba}_{0.72}\text{K}_{0.28}\text{Fe}_2\text{As}_2$ single crystal from the same batch and

obtained similar results as for the first crystal. In addition to our $\text{Ba}_{0.72}\text{K}_{0.28}\text{Fe}_2\text{As}_2$ single crystal, we recently have also studied V - I characteristics of electron-doped $\text{Ba}(\text{Ni}_{0.1}\text{Fe}_{0.9})_2\text{As}_2$ single crystals and found that the V - I characteristics at high voltages were similar in shape to those shown in Figs. 2 and 3.

V. CONCLUSION

We have investigated experimentally and by model calculations the V - I characteristics of a $\text{Ba}_{0.72}\text{K}_{0.28}\text{Fe}_2\text{As}_2$ superconducting single crystal slightly below the transition temperature, in different magnetic fields applied along the crystallographic c direction. Because of self-heating, V - I characteristics at lower temperatures were not investigated. Our theoretical model describes the motion and hopping of flux-line bundles under the influence of an electrical drive current where the bundle motion is strongly damped by the dissipative resistance of the material. The cause for the thermally assisted flux-line bundle hopping is the Johnson white-noise current in the two-band resistances $R_n^{(S)}$ and $R_n^{(L)}$. The main equation, Eq. (7), of our model resembles the equation of a RSJJ but with a different noise term. For drive currents much smaller than the depinning current, our model is the same as the TAFF model. Our model describes remarkably well our measured V - I characteristics over a wide current and magnetic field range and indicates that the contribution from a Bardeen-Stephen flux-flow resistance is small. In particular, the model allows us to extract from the data (a) the depinning current density J_c , (b) the barrier height U_0 of the pinning potential, and (c) the dissipative resistance R . The product $V_b a_h$ between bundle volume V_b and hopping distance a_h can be determined from J_c and U_0 as a function of the magnetic field B . The different slopes observed in plots of $\log(V_b a_h)$ versus $\log B$ reveal different regimes of the flux-line bundle dynamics, which can be used to estimate the average distance between pins.

ACKNOWLEDGMENTS

The authors would like to thank G. L. Sun, D. L. Sun, and C. T. Lin from MPI, Stuttgart, Germany, for supplying us with a $\text{Ba}_{0.72}\text{K}_{0.28}\text{Fe}_2\text{As}_2$ single crystal. This work was partially supported by the Australian Research Council through Discovery Projects DP1094073 and DP120100095.

*Corresponding author: karl.muller@csiro.au

¹P. W. Anderson, *Phys. Rev. Lett.* **9**, 309 (1962); P. W. Anderson and Y. B. Kim, *Rev. Mod. Phys.* **36**, 39 (1964).

²Y. Yeshurun and A. P. Malozemoff, *Phys. Rev. Lett.* **60**, 2202 (1988).

³A. P. Malozemoff, L. Krusin-Elbaum, D. C. Cronmeyer, Y. Yeshurun, and F. Holtzberg, *Phys. Rev. B* **38**, 6490 (1988).

⁴T. T. M. Palstra, B. Batlogg, L. F. Schneemeyer, and J. V. Waszczak, *Phys. Rev. Lett.* **61**, 1662 (1988).

⁵M. Tinkham, *Phys. Rev. Lett.* **61**, 1658 (1988).

⁶C. W. Hagen and R. Griessen, *Phys. Rev. Lett.* **62**, 2857 (1989).

⁷V. B. Geshkenbein, M. V. Feigel'man, A. I. Larkin, and V. M. Vinokur, *Physica C* **162**, 239 (1989).

⁸P. H. Kes, J. van den Berg, C. J. van der Beek, and J. A. Mydosh, *Supercon. Sci. Technol.* **1**, 242 (1989).

⁹M. P. A. Fisher, *Phys. Rev. Lett.* **62**, 1415 (1989).

¹⁰V. M. Vinokur, M. V. Feigel'man, V. B. Geshkenbein, and A. I. Larkin, *Phys. Rev. Lett.* **65**, 259 (1990).

¹¹T. T. M. Palstra, B. Batlogg, R. B. van Dover, I. F. Schneemeyer, and J. V. Waszczak, *Phys. Rev. B* **41**, 6621 (1990).

¹²D. S. Fisher, M. P. A. Fisher, and D. A. Huse, *Phys. Rev. B* **43**, 130 (1991).

- ¹³G. Blatter, M. V. Feigel'man, V. B. Geshkenbein, A. I. Larkin, and V. M. Vinokur, *Rev. Mod. Phys.* **66**, 1125 (1994), and the references therein.
- ¹⁴E. H. Brandt, *Rep. Prog. Phys.* **58**, 1465 (1995).
- ¹⁵S. N. Gordeev, A. P. Rassau, R. M. Langan, P. A. J. de Groot, V. B. Geshkenbein, R. Gagnon, and L. Taillefer, *Phys. Rev. B* **60**, 10477 (1999).
- ¹⁶H. C. Yang, L. M. Wang, and H. E. Horng, *Phys. Rev. B* **59**, 8956 (1999).
- ¹⁷J. Kierfeld, H. Nordborg, and V. M. Vinokur, *Phys. Rev. Lett.* **85**, 4948 (2000).
- ¹⁸D. Ravelosona, J. P. Contour, and N. Bontemps, *Phys. Rev. B* **61**, 7044 (2000).
- ¹⁹M. Andersson, A. Rydh, and O. Rapp, *Phys. Rev. B* **63**, 184511 (2001).
- ²⁰J. Figueras, T. Puig, and X. Obradors, *Phys. Rev. B* **67**, 014503 (2003).
- ²¹J. Jaroszynski, F. Hunte, L. Balicas, Y. J. Jo, I. Raičević, A. Gurevich, D. C. Larbalestier, F. F. Balakirev, L. Fang, P. Cheng, Y. Jia, and H. H. Wen, *Phys. Rev. B* **78**, 174523 (2008).
- ²²R. Prozorov, N. Ni, M. A. Tanatar, V. G. Kogan, R. T. Gordon, C. Martin, E. C. Blomberg, P. Prommapan, J. Q. Yan, S. L. Bud'ko, and P. C. Canfield, *Phys. Rev. B* **78**, 224506 (2008).
- ²³Y. Liu, S. Chai, H.-J. Kim, G. R. Stewart, K. H. Kim, Z.-A. Ren, and Z.-X. Zhao, *J. Korean Phys. Soc.* **55**, L383 (2009).
- ²⁴Y. Z. Zhang, R. A. Ren, and Z. X. Zhao, *Supercon. Sci. Technol.* **22**, 065012 (2009).
- ²⁵M. Shahbazi, X. L. Wang, C. Shekhar, O. N. Srivastava, and S. X. Dou, *Supercon. Sci. Technol.* **23**, 105008 (2010).
- ²⁶M. A. Tanatar, N. Ni, S. L. Bud'ko, P. C. Canfield, and R. Prozorov, *Supercon. Sci. Technol.* **23**, 054002 (2010).
- ²⁷X. L. Wang, S. R. Ghorbani, S.-I. Lee, S. X. Dou, C. T. Lin, T. H. Johansen, K.-H. Müller, Z. X. Cheng, G. Peleckis, M. Shabazi, A. J. Qviller, V. V. Yurchenko, G. L. Sun, and D. L. Sun, *Phys. Rev. B* **82**, 024525 (2010).
- ²⁸H. Ding, P. Richard, K. Nakayama, K. Sugawara, T. Arakane, Y. Sekiba, A. Takayama, S. Souma, T. Sato, T. Takahashi, Z. Wang, X. Dai, Z. Fang, G. F. Chen, J. L. Luo, and N. L. Wang, *Europhys. Lett.* **83**, 47001 (2008).
- ²⁹R. Khasanov, D. V. Evtushinsky, A. Amato, H.-H. Klauss, H. Luetkens, Ch. Niedermayer, B. Büchner, G. L. Sun, C. T. Lin, J. T. Park, D. S. Inosov, and V. Hinkov, *Phys. Rev. Lett.* **102**, 187005 (2009).
- ³⁰N. Nakamura, M. Machida, T. Koyama, and N. Hamada, *Physica C* **470**, 1066 (2010).
- ³¹J. Kacmarcik, C. Marcenat, T. Klein, Z. Pribulova, C. J. van der Beek, M. Konczykowski, S. L. Budko, M. Tillman, N. Ni, and P. C. Canfield, *Phys. Rev. B* **80**, 014515 (2009).
- ³²D. L. Sun, Y. Liu, and C. T. Lin, *Phys. Rev. B* **80**, 144515 (2009).
- ³³R. F. Voss, *J. Low. Temp. Phys.* **42**, 151 (1981).
- ³⁴V. Ambegaokar and B. I. Halperin, *Phys. Rev. Lett.* **22**, 1364 (1969).
- ³⁵M. W. Coffey and J. R. Clem, *Phys. Rev. Lett.* **67**, 386 (1991).
- ³⁶J. Goryo and H. Matsukawa, *J. Phys. Soc. Jpn.* **74**, 1394 (2005).
- ³⁷K. K. Likharev, *Dynamics of Josephson Junctions and Circuits* (Gordon and Breach, New York, 1986), p. 117.
- ³⁸H. Yang, H. Luo, Z. Wang, and H.-H. Wen, *Appl. Phys. Lett.* **93**, 142506 (2008).
- ³⁹S. Salem-Sugui Jr., L. Ghivelder, A. D. Alvarenga, L. F. Cohen, K. A. Yates, K. Morrison, J. L. Pimentel Jr., H. Luo, Z. Wang, and H.-H. Wen, *Phys. Rev. B* **82**, 054513 (2010).
- ⁴⁰D. L. Sun, Y. Liu, and C. T. Lin, *Phys. Rev. B* **80**, 144515 (2009).
- ⁴¹V. A. Gasparov, *J. Exp. Theor. Phys.* **11**, 313 (2010).
- ⁴²W. K. Yeoh, B. Gault, X. Y. Cui, C. Zhu, M. P. Moody, L. Li, R. K. Zheng, W. X. Li, X. L. Wang, S. X. Dou, G. L. Sun, C. T. Lin, and S. P. Ringer, *Phys. Rev. Lett.* **106**, 247002 (2011).
- ⁴³S. Demiris, C. J. van der Beek, Y. Fasano, N. R. Cejas Bolecek, H. Pastoriza, D. Colson, and F. Rullier-Albenque, *Phys. Rev. B* **84**, 094517 (2011).
- ⁴⁴A. I. Larkin and Yu. N. Ovchinnikov, *J. Low Temp. Phys.* **34**, 409 (1979).